Dominant Conformation of Valsartan in Sodium Dodecyl Sulfate Micelle Environment

Fang Li,[†,‡,§] Lingyun Wang,[†,‡,§] Nan Xiao,[†,‡] Minghui Yang,[†] Ling Jiang,*[,†] and Maili Liu[†]

Wuhan Center for Magnetic Resonance, State Key Laboratory of Magnetic Resonance and Atomic and Molecular Physics, Wuhan Institute of Physics and Mathematics, Chinese Academy of Sciences, Wuhan, 430071, People's Republic of China, and Graduate School, Chinese Academy of Sciences, Beijing 100049, People's Republic of China

Received: September 16, 2009; Revised Manuscript Received: December 13, 2009

The interaction of valsartan (VST), a novel antihypertensive drug, with sodium dodecyl sulfate (SDS) micelles has been investigated using Nuclear Magnetic Resonance (NMR) spectroscopy and Molecular Dynamics (MD) simulation. VST has two conformations in solution, exchanging slowly on the NMR time scale via the *trans*/*cis* (conformer A/B) isomerization of the amide bond. It is suggested that drugs in the sartan class incorporate and diffuse into biological membranes before they interact with AT_1 receptors. SDS is used to mimic the membrane environment to characterize two VST conformers. ^{1}H NMR chemical shift analysis, proton relaxation rates, and self-diffusion coefficient measurements suggest that conformer A has a higher binding affinity to SDS and is the dominant conformer distributed in the SDS micelles. The location of VST in the micelles is determined by NOE measurements and by the MD simulation, showing that the butyl chain and biphenyl groups of VST interact with the alkyl group of SDS through hydrophobic interactions. Preferable binding free energy is found for conformer A by the MD simulation, which demonstrates that the relatively concentrated hydrophobic surface of conformer A is responsible for its higher affinity to the micelles. Our results are in good agreement with a recent simulation of VST bound onto the AT_1 receptor by Potamitis et. al (*J. Chem. Inf. Model.* **2009**) who demonstrate that conformer A (*trans* conformation in their definition) is the one binding to the receptor. The results presented in our study suggest that the biological membrane plays an essential role in stabilization of the active state of VST. Thus, understanding the interactions between the sartan drugs and the membrane environment should facilitate the studies of the functional mechanism of these compounds with their receptor and provide insight on the development of new approaches for drug discovery.

Introduction

According to the World Health Organization, high blood pressure, also known as hypertension, is the most prevalent risk factor for cardiovascular diseases. It affects approximately 26% of the adults in 2000 and has been estimated to be responsible for at least 7 million deaths each year.[1] Furthermore, researchers predict that by 2025, 29% (over 1.5 billion adults) of the number of people worldwide will be affected by this serious condition.[2] For this reason, there is a great need for novel drugs that regulate the blood pressure with longer duration of action. Valsartan (VST), as a sartan drug, acts on the AT_1 receptor (angiotensin II receptor, type 1) to block the effect of angiotensin II in the renin−angiotensin system cascade.[3] It has been shown that VST has the best in vitro and in vivo activity in a series of antagonists compared with losartan as the primary structure.[4] The AT_1 receptor is a seven transmembrane G protein-coupled receptor.[5−7] It is reported that sartan drug interacts with the amino acids in the transmembrane domains of the AT_1 receptor and occupies space among the seven helixes, preventing the binding of angiotensin II.[8,9] Therefore, studies on the conformation of VST are of vital importance for drug design and hence the development of fundamental treatment for cardiac hypertrophy and heart failure.

In our previous work, we found that VST has two distinct conformational isomers in methanol, which exchange slowly on the NMR (Nuclear Magnetic Resonance) time scale with similar concentrations via rotation about the C(O)−N bond.[10] VST can be therefore classified into conformer A and B based on the hindered *cis*/*trans* isomerization of the amide bond. Recently, Potamitis and co-workers demonstrated the existence of *cis*/*trans* isomerization of VST in DMSO, which is consistent with our findings.[11] They have explored the conformational properties of VST by NMR spectroscopy and Molecular Dynamics (MD) simulation. The simulation revealed that two acidic groups of VST play an important role in binding to the AT_1 receptor site models, and the majority of docked poses adopted a *trans* conformation. They defined the dihedral angle in a different way, and the *trans* isomer is the same as conformer A in our studies. In the precious works of Mavromoustakos's group, the authors suggested that the sartan drug bound onto the receptor after its insertion and diffusion through membrane bilayers.[12,13] A question arises, however, as to whether or not VST adopts a dominant conformation in the cell membrane before it reaches the receptor. Herein, we investigated the structural characterization of VST in a mimic membrane using NMR spectroscopy and MD simulation to provide information on how sartan drugs interact with the membrane.

Micelles, dynamic nanostructures of surfactant molecules, have the capability to solubilize a wide variety of organic molecules with different polarities and hydrophobicities. Sodium dodecyl sulfate (SDS) is often used to solubilize small mem-

* To whom correspondence should be addressed. E-mail: lingjiang@wipm.ac.cn.
† Wuhan Institute of Physics and Mathematics.
‡ Graduate School, Chinese Academy of Sciences.
§ These authors contributed equally to this work.

10.1021/jp908958k
Published on Web 02/04/2010

brane proteins or to mimic the membrane environment in the conformational analysis of bioactive peptides.[14−17] As one of the most common membrane-mimicking aqueous media compatible with NMR studies, SDS forms stable micelles with small aggregation numbers and undergoes relatively rapid reorientation in aqueous solution.[18] It provides us with an excellent opportunity to investigate the characterization of two conformers of VST in micelles and to ultimately analyze their distribution properties in this membrane-like environment.

NMR spectroscopy can provide information at molecular and atomic levels under physiological or "near-physiological" conditions. As a unique tool, NMR has been widely used to investigate drug−protein interaction and to derive information of binding site and affinity, conformation, and dynamics in a noninvasive manner. Such information is included in NMR observable parameters, such as chemical shift,[19−22] relaxation time,[23−26] self-diffusion coefficient,[22,27−29] and Nuclear Overhauser Effects (NOE).[30,31] In this article, we use these NMR techniques to investigate the structural characterization of VST in SDS. Molecular dynamics simulation has been also implemented and provided evidence that conformer A has a higher binding affinity to SDS micelles, which gives vital evidence in deducing that conformer A would keep a higher concentration than conformer B in a biological membrane system.

Experimental Methods

Sample Preparation. Sodium dodecyl sulfate (SDS, over 99% purity) was purchased from Alfa Aesar (Johnson-Matthey Company). Hexadecyltrimethylammonium bromide (CTAB, 99%) was bought from Acros Organics (New Jersey, USA). D_2O (99.8% *d*, Acros Organics) was used as the solvent in these studies. Valsartan, (*S*)-*N*-valeryl-*N*-((2′-(1*H*-tetrazol-5-yl)-biphenyl-4-yl)-methyl)-valine, was purified as described previously.[32]

Two groups (G1 and G2) of VST samples were prepared in 0.02 M phosphate buffer (pD 7.40) in D_2O. Samples in group G1 only contained VST. Samples in group G2 contained VST and 200 mM SDS. For each group, the concentration of VST was varied: 1.0, 2.0, 3.0, 4.0, 5.0, 6.0, 7.0, 8.0, 10.0, 12.0, and 15.0 mM. A sample containing 200 mM SDS but without VST was prepared to serve as the control. Another sample consisted of 15 mM VST, and 10 mM CTAB was also prepared in the same buffer.

NMR Spectroscopy. All NMR experiments were performed at 298 K on a Bruker AVANCE-600 instrument equipped with a 5 mm triple-resonance cryoprobe, operating at a proton frequency of 600.13 MHz. Single-pulse ^{1}H NMR spectra were acquired using a solvent presaturation sequence with a spectra width of 8000 Hz, 64 scans, and 32k data points. Longitudinal relaxation times (T_1) were determined by an inversion recovery sequence, and transversal relaxation times (T_2) were determined by a CPMG pulse sequence. The self-diffusion coefficients were measured using a double longitudinal eddy-current delay experiment with bipolar gradient pulses to eliminate the influence of thermal convection.[33] The effective diffusion time is 400 ms. NOESY spectra were acquired by a standard water suppressed NOESY sequence, with 2048 (F2) × 256 (F1) complex data points with 32 scans at a mixing time of 200 ms. The time domain data of NOESY spectra were weighted using a sine-bell window function and zero-filled to 2048 (F2) × 1024 (F1) before Fourier transformation.

Model Construction and Molecular Dynamics Simulation. All MD Simulations were performed using the AMBER9.0 package,[34] and the GAFF force field[35] was used to describe molecular interactions. Initially, a sodium dodecyl sulfate (SDS) micelle was constructed with 60 SDS molecules. It is the aggregation number of SDS reported at room temperature[36] and is a feasible size to mimic the physical properties of the micelle.[37] The micelle was placed in a truncated octahedron box filled with TIP3P[38] water molecules. The size of the water sphere was chosen so that the distance between every atom in the micelle and the boundary of the water was at least 10 Å. In addition, Na^+ counterions were added to balance the negative charges of the sulfate groups. The entire micelle/water assembly was subsequently equilibrated by a 5000-step energy minimization and a 2 ns MD simulation under NPT conditions.

SCHEME 1: Thermodynamic Cycle Used in Free Energy Calculation[a]

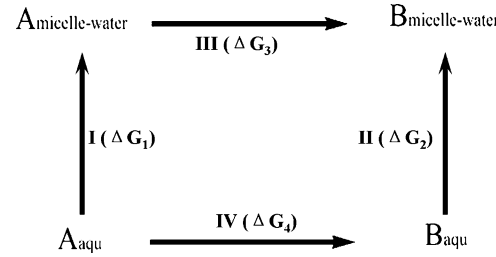

[a] The relative binding free energy can be calculated as: $\Delta\Delta G_{(A\rightarrow B)} = \Delta G2 - \Delta G1 = \Delta G3 - \Delta G4$.

In the next step, the VST conformers were, respectively, placed in the simulation box with their mass centers coinciding with that of the micelle (Supporting Information, Figure S1). Owing to spherical symmetry of the micelle, the orientation of VST will not impact its diffusion.[39] The geometries of VST were taken from our previous work,[10] and the partial charges (Supporting Information, Figure S2) were obtained using HF/6-31G* single-point calculation with the Gaussion03 suit of programs[40] and the restrained electrostatic potential (RESP) method.[41]

Subsequently, two separate MD simulations were carried out. For each of these calculations, the system contains one of the VST conformer and one SDS micelle. The system was first minimized for 10 000 steps (5000 steps in steepest descent method and then 5000 steps in conjugate gradients method) under weak harmonic constraints on VST with spring constants of 10 kcal/(mol·Å^2). After another 10 000-step minimization with all constraints switched off, the system was gradually heated to 298 K in 50 ps in NVT ensemble and then subjected to NPT dynamics (pressure $P = 1$ atm and temperature $T =$ 298 K) for 21 ns. The pressure was adjusted by isotropic position scaling, and the Berendsen thermostat[42] (weak-coupling method) was used to control the temperature constant. Periodic boundary conditions along with the Particle Mesh Ewald (PME)[43] method was used to treat long-range electrostatic interactions, and the cutoff for the nonbonded interactions is 15 Å. The SHAKE algorithm[44] was employed to constrain all bonds involving hydrogen atoms. The time step was 2 fs, and the trajectories were collected every 1 ps. The analysis of the trajectories was performed using the PTRAJ program in AMBER 9.0, and the VMD program[45] was used in the visualization of the configuration of VST in SDS micelle.

Free Energy Calculation. The relative binding free energy of the two VST conformers with SDS micelle can be obtained through the thermodynamic cycle[46] depicted in Scheme 1, where $\Delta G1$ and $\Delta G2$ refer to the binding free energies of VST (conformer A and B, respectively) with SDS and $\Delta G3$ and $\Delta G4$ are the isomerization free energies of conformer A to conformer

B in SDS micelle/water and aqueous solution, respectively. The relative binding free energy stands for the difference between the binding free energies of two conformers, $\Delta\Delta G_{(A\rightarrow B)} = \Delta G_{(binding,\ B)} - \Delta G_{(binding,\ A)} = \Delta G2 - \Delta G1$. Free energy is a state function, which means $\Delta G2 - \Delta G1 = \Delta G3 - \Delta G4$. That is to say, the relative binding free energy can be obtained by $\Delta\Delta G_{(A\rightarrow B)} = \Delta G3 - \Delta G4$.

Umbrella sampling[47] simulations were carried out to obtain the isomerization free energies, $\Delta G3$ and $\Delta G4$. In the simulations, the change of dihedral angle τ_5 (from conformer A to conformer B) was chosen as the reaction coordinate. The geometry of conformer A of VST obtained from our previous work[10] was solvated by TIP3P water molecules and taken as the starting structure in aqueous solution, while the initial structure of VST in SDS micelle/water was obtained from the equilibrated conformation of conformer A at 20 ns in MD simulation. The dihedral angle τ_5 was harmonically restrained from 0° to 180° at 10° increments, which resulted in 19 separate MD window runs in either solvent condition. The harmonic constraint potential $U_c(x) = f^*(x - x_0)^2$ was introduced to restrain the dihedral angle x (i.e., τ_5) to a limited region, using a force constant of 0.05 kcal/(mol·deg^2). For each window, 9.5 ns MD simulations were carried out for VST in micelle/water and 5 ns in aqueous solution. Within each window, the biased distribution $P(x)$ of the dihedral angle x was calculated and converted to a PMF (potential of mean force) $w(x)$ according to eq 1[48]

$$w(x) = -kT \ln P(x) - U_c(x) + C \qquad (1)$$

where k is the Boltzmann constant; T is the temperature; U_c is the constraint potential; and C is an arbitrary constant. The reaction coordinate was recorded every 2 fs. The final free energy profile was calculated with the weighted histogram analysis method[49,50] (WHAM) implemented in the WHAM program,[51] and the Monte Carlo bootstrap analysis was used to estimate the corresponding error bar.

Results and Discussions

Chemical structure and the numbering system of VST are shown in Scheme 2. All of the proton resonances of VST in the absence and presence of SDS are assigned and grouped into conformer A and B based on our previous published data.[10] The structural difference between conformer A and B lies in their distinct dihedral angle τ_5 defined in Scheme 2; namely, τ_5 of A is 1.6°, while B is 174.2°.

NMR Parameter Perturbations by the Addition of SDS. Figure 1 shows the expanded ^{1}H NMR spectra of VST at a concentration of 15 mM in the absence (a) and presence (b) of 200 mM SDS. In the free VST solution, the H4 methylene protons of two conformers are both magnetically nonequivalent. When 200 mM SDS was added, chemical shift drifting and line broadening can be clearly observed. The two H4 peaks of conformer A, for instance, start to merge, and those of conformer B even become magnetically equivalent. The merging and broadening effects of resonance peaks indicate their interactions with SDS.

The chemical shifts of some isolated protons are illustrated in Figure 2. They are referenced to the residual HOD signal inside the samples. There are no perceivable changes of proton chemical shifts with the variation of VST concentration since the slopes of all the fitting lines are less than 1.3×10^{-3}. The shift is mainly caused by the variation of pD values. The pD value of the phosphate buffer we used is 7.40, while the dissociation constants of the acidic groups in VST are much lower; i.e., the pK_a of the carboxyl group is 3.90, and that of the amidocyanogen is 4.73.[52] The increasing VST concentration makes the pD value of the solution vary, then slightly influences the proton chemical shifts.

SCHEME 2: Molecular Structures of Valsartan, SDS, and CTAB[a]

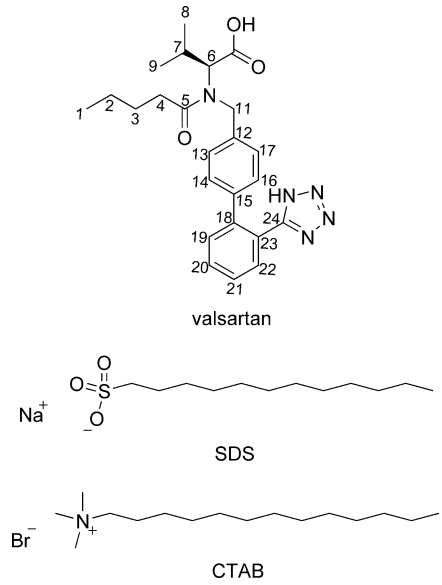

[a] Five dihedral angles are defined as τ_1 = C18−C23−C24−N(H), τ_2=C19−C18−C15−C14, τ_3=C13−C12−C11−N, τ_4=C12−C11−N−C6, and τ_5 = C6−N−C5−O.

The addition of SDS causes downfield shifts of VST resonances. The perturbations of the phenyl protons H14/16 and methylene protons H4 indicate that the aromatic and aliphatic parts are both involved in the interaction. The perturbations of H4 protons for conformers A and B have the same trends; however, the magnitudes are slightly different. It is likely that the H4 protons of conformers A and B experience different chemical environments in the SDS micelles.

The interaction between VST and SDS can be further confirmed by measurements of relaxation times (Supporting Information, Tables S1 and S2). In both groups of samples, relaxation times are not influenced by the VST concentration. Addition of SDS does not change the longitudinal relaxation times of VST protons very much but reduces their transverse relaxation times significantly, indicating the restricted movement of VST molecules in the presence of micelles. Additionally, conformational heterogeneity is found for VST in the micelles. The changes of T_2 values of H4 protons in conformer A, for instance, are much larger than those in conformer B, indicating a stronger interaction between conformer A and SDS.

Higher Affinity of Conformer A to SDS Micelles. The self-diffusion coefficients (D) measured for both groups of samples are illustrated in Figure 3. For each conformer, the H4 protons which give the most isolated peaks are chosen to calculate the D value. All of the self-diffusion coefficients are not sensitive to VST concentration, indicating no self-aggregations happen while increasing the amount of VST. Although the samples were prepared in 99.8% D_2O, there are still residual HOD signals observed in the ^{1}H NMR spectra without water suppression. The signals are then used to measure the self-diffusion effects of the solvents. In Figure 3(a), the mean D value of residual HOD in samples G1 is 1.90×10^{-9} m^2/s, while in the presence

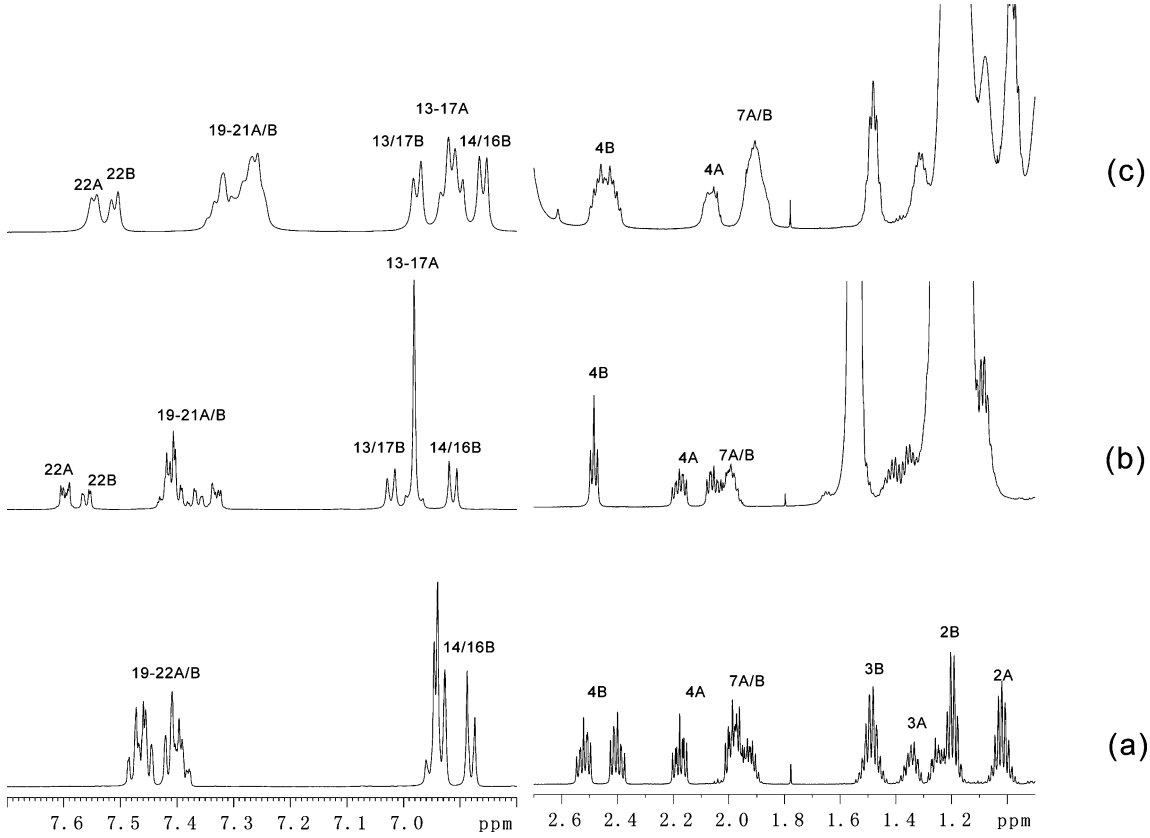

Figure 1. ^{1}H NMR spectra of 15.0 mM VST in phosphate buffer (a), in 200 mM SDS (b), and in 10 mM CTAB (c).

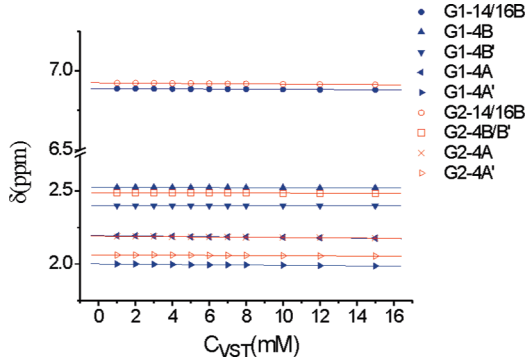

Figure 2. ^{1}H chemical shifts of two conformers in group G1 (blue) and group G2 (red) as a function of VST concentrations.

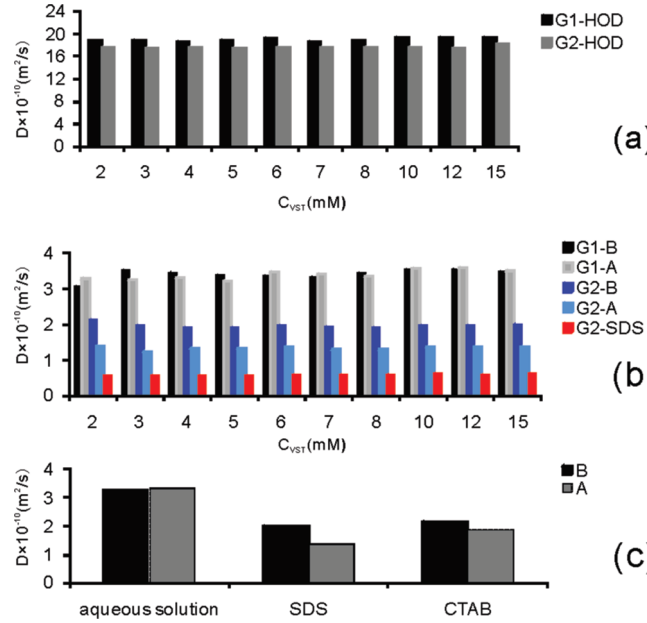

Figure 3. Variations of self-diffusion coefficients of (a) HOD and (b) VST in samples G1 and G2 as a function of VST concentrations. The self-diffusion coefficients of SDS in G2 are shown in (b) as red bars. (c) The self-diffusion coefficients of 15 mM VST in phosphate buffer, 200 mM SDS, and 10 mM CTAB.

of SDS, it reduces to 1.77×10^{-9} m^2/s because of the increased viscosity of the solvents. In Figure 3(b), no big difference is found for the mean D values of two conformers in the phosphate buffer, which are both about 3.55×10^{-10} m^2/s. In the presence of SDS, the mean D values drop to 1.34×10^{-10} and 1.97×10^{-10} m^2/s for conformer A and B, respectively. The values are larger than that of the SDS (0.59×10^{-10} m^2/s). This is because the free and bound forms of VST are exchanging in solution. The self-diffusion coefficient of VST should be an apparent coefficient that is a fraction-weighted average of the free and bound states of two isomers. The self-diffusion coefficient of the bound VST is expected to be similar to that of the SDS micelles. Qualitatively speaking, the lower self-diffusion coefficient implies that a larger proportion of conformer A is in the bound state. In other words, conformer A has a higher binding affinity to the micelles.

Concentration ratios of conformer A to B in different samples are obtained by peak integration and shown in Figure 4. It is obvious that for samples G1 the values of A:B are almost the same, which are around 0.88. For the samples of VST containing SDS, the values are almost doubled. They slightly decrease from 1.59 to 1.51 as the VST concentration increases from 1 to 5 mM and then fluctuate around 1.50 as VST concentration increases. It further confirms that conformer A has a higher binding affinity to SDS.

Hydrophobic Interaction between VST and SDS. In the phosphate buffer at pD 7.40, VST exists in an ionic state, which

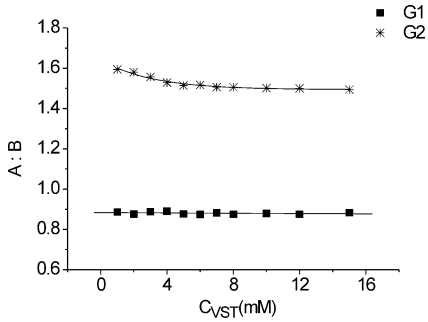

Figure 4. Concentration ratio of conformer A to B in samples G1 (■) and G2 (∗) as a function of VST concentrations.

has distinct polar and nonpolar parts. SDS is an anionic surfactant. There could be electrostatic or hydrophobic interactions between them. To examine the binding mechanism, a cationic surfactant CTAB is chosen, and a set of samples containing VST, VST−SDS, or VST−CTAB at the VST concentration of 15 mM are investigated. The addition of CTAB or SDS causes many similar changes in the ^{1}H NMR spectra, such as the merging of magnetically nonequivalent protons, the overlapping signals in aromatic region, and the increased A:B values (Figure 1(c)). These changes suggest that VST interacts with two kinds of micelles in a similar fashion.

The self-diffusion coefficient of VST can be used to study the global behaviors of different conformers. Compared to the *D* value in 15 mM VST solution (Figure 3(c)), the addition of 200 mM SDS causes 59% decrease of the *D* value for conformer A and 39% decrease for conformer B, respectively. In the sample consisting of 15.0 mM VST and 10 mM CTAB, the decreasing percentages of *D* values for conformer A and B are 44% and 34%, respectively. That is to say, like SDS, CTAB interacts with both conformers and slows down their self-diffusion effects. At the same time, the *D* value of conformer A reduces more than that of conformer B because of its higher affinity to the micelles. All these results indicate that two conformers interact not only with the negatively charged SDS micelles but also with the positively charged CTAB micelles. Therefore, the hydrophobic interaction is the dominant effect in the solvent. It can be confirmed by the upfield shifts of phenyl protons in sample G2 and the following NOE analyses.

Direct Evidence of Interaction between VST and SDS. The nuclear overhauser effect (NOE) can provide a unique spatial relationship between two nuclei of less than 5 Å in distance. The intensity of the cross-peak in the NOE correlation spectrum (NOESY) is proportional to inverse six order of internuclear distance. The approach is adopted to characterize the interaction between VST and SDS. Figure 5 shows the expansions of NOESY spectra of VST in phosphate buffer, SDS, and CTAB,

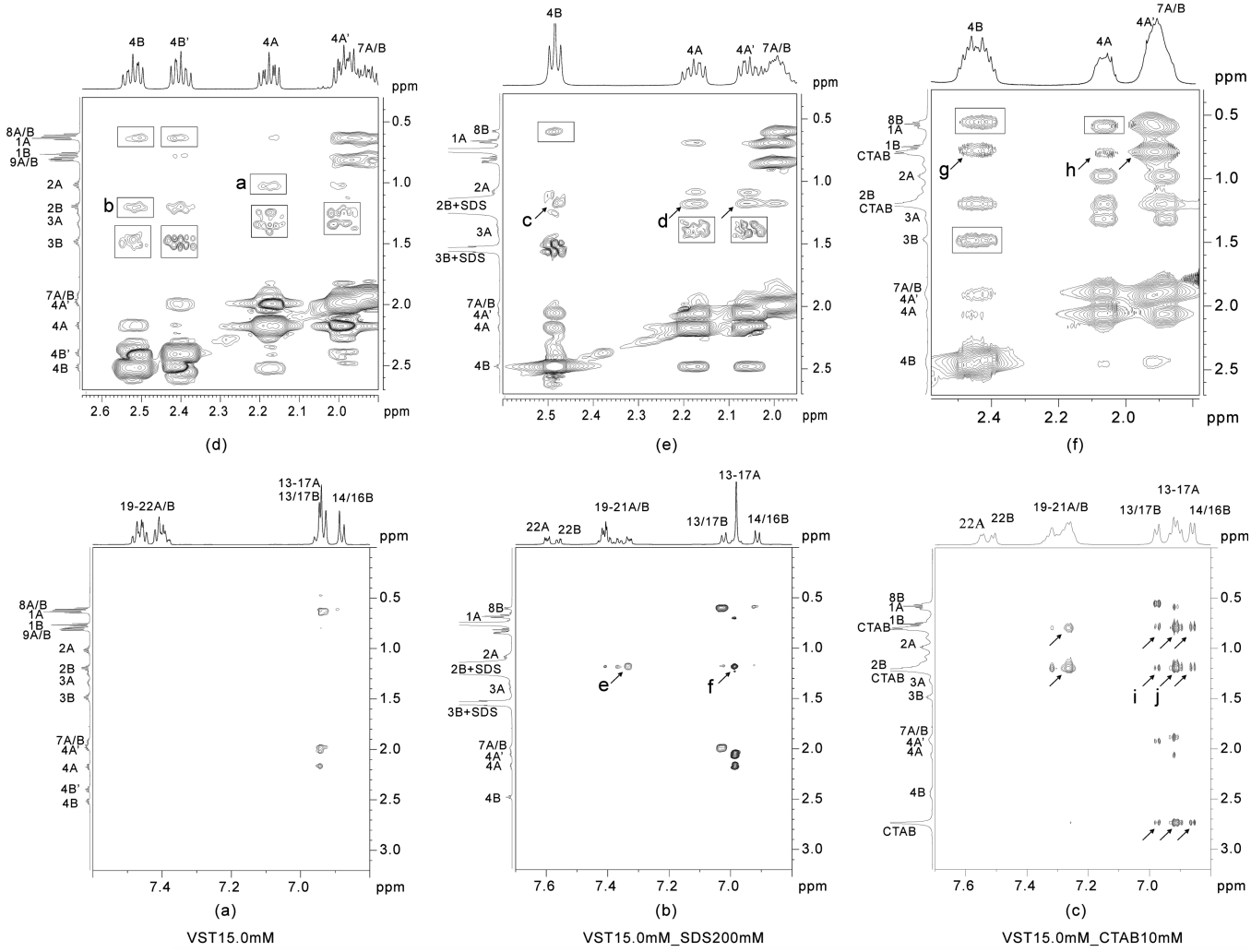

Figure 5. Expansions of NOESY spectra of 15.0 mM VST in phosphate buffer (a, d), in 200 mM SDS (b, e), and in 10 mM CTAB (c, f). The mixing time is 200 ms. Intramolecular cross peaks are indicated with rectangles, and intermolecular cross peaks are indicated with arrows.

respectively. The bottom three spectra show NOE cross peaks between the alkyl chain of SDS or CTAB and the biphenyl groups of VST for both conformers. The upper three spectra show the existence of NOE cross peaks between the alkyl chain of SDS or CTAB and the butyl group of two VST conformers.

In Figure 5(a) and (d) where VST is in its free form, there are NOE peaks between protons which are adjacent or close in space. These intramolecular NOEs are labeled with rectangles. For example, peaks a and b indicate the NOE relationship between H4 and H2 of conformer A and B, respectively. After the addition of detergents, the intramolecular NOE peaks can still be seen. Meanwhile, intermolecular cross peaks between detergents and VST conformers appear which are marked with arrows. In Figure 5(b), peaks e and f show that the aliphatic chain of SDS interacts with the aromatic rings of VST for both conformers. In Figure 5(e), peaks c and d indicate that the aliphatic chain of SDS is close to H4 of VST for both conformers, while in Figure 5(c) and (f), peaks i, j, g, and h show the interactions between the aliphatic chain of CTAB and VST for both conformers. This direct NOE evidence indicates that VST diffuses into the micelles and the nonpolar parts including butyl and biphenyl groups insert into the hydrophobic center of the mimic membrane.

Molecular Dynamics Simulation of VST in SDS Micelle. NMR experiments provide strong evidence that conformer A has a higher affinity when it interacts with SDS. Investigations of the VST geometry by MD simulation would reveal the structural determinants that govern the binding mechanism, thus establishing an excellent foundation for the understanding of the finer details in the interaction process.

Two MD simulations were carried out for each VST conformer in a micelle consisting of 60 SDS molecules. The distances between the mass center of VST and that of the SDS micelle are measured to determine if the conformer has diffused to the interfacial region between the micelle and water. The diffusion occurred within 3 ns for conformer A and 2 ns for conformer B (Supporting Information, Figure S3). The values of radius of gyration (Rg) of both systems are 14.7 ± 0.5 Å, which are in good agreement with an experimental value[53] of 15.4 Å for a lithium dodecyl sulfate (LDS) micelle and a theoretical value of 15.5 Å for a SDS micelle.[54] The radial distribution function (RDF) of sodium to the sulfate head groups is very similar to the result of Bruce,[55] confirming that the overall micelle geometry predicted by our simulation approach is reliable and comparable to other atomistic simulation results (Supporting Information, Figure S4).

Root-mean-square deviations (rmsd) and root-mean-square fluctuations (rmsf) of VST during the simulations are both calculated relative to its initial structure[10] (Supporting Information, Figure S5). The rmsd of conformer A fluctuates between 1 and 3 Å during the entire 21 ns simulation; however, the rmsd of conformer B remains at 1.5 Å for the first 11 ns, then reaches to 3 Å and keeps stable at this level for the remainder of the simulation. The change of rmsd indicates that conformer B could have a conformational change at 11 ns. The larger rmsf of conformer B at the carbonyl group, C11 and C12, also suggests that conformer B is more flexible.

Dihedral angles related to C11 and C12 of VST are analyzed and shown in Figure 6. Notably, it reveals that conformer B has major changes in dihedral angle τ_3 and τ_4 after 11 ns (Figure 6(a), 6(b)), corresponding to the time of changes in rmsd value, while conformer A does not show big differences in τ_3 and τ_4. The dihedral angle τ_5 (Figure 6(c)) which distinguishes the

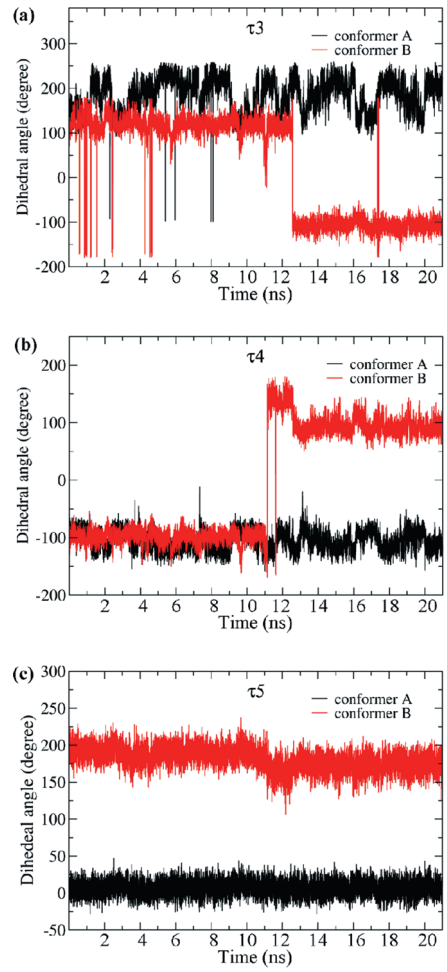

Figure 6. Time profiles of dihedral angles (a) τ_3 (C13−C12−C11−N), (b) τ_4 (C12−C11−N−C6), and (c) τ_5 (C6−N−C5−O) for conformer A (black lines) and conformer B (red lines).

conformers remains constant for conformer A but slightly reduces 7° at about 11 ns for conformer B.

Spatial Structure Comparison of Two Conformers. To get insight into the conformational changes of VST, snapshots at the end of the simulations are illustrated in Figure 7. The conformations of VST calculated in our previous published data[10] are also provided for comparison. It can be clearly seen that, in vacuum (Figure 7(b) and 7(d)), two conformers have the same structural characterizations except a different dihedral angle τ_5. The rotation of τ_5 determines the orientation of the butyl group relative to the biphenyl ring.

In SDS micelles, two conformers have similar final binding configurations (Figure 7(a) and 7(c)). The hydrophobic butyl chain and biphenyl ring are anchored into the SDS micelle core, while the tetrazole ring and carboxyl group are exposed to the aqueous solution. This is consistent with the chemical shift changes and NOE analyses in NMR experiments. Since the hydrophobic interaction has been identified as the dominant effect in the binding mode and the butyl chain and biphenyl ring are the main hydrophobic segments in VST, a parameter θ, which is defined as the angle between atoms C1−N−C21 in Figure 7(d), is used to characterize the hydrophobic surface of two conformers in SDS. Figure 7(e) shows the probability distribution of angle θ. Larger values are found for conformer B indicating its relative dispersive hydrophobic surface. To characterize the binding affinity, radial distribution functions (RDFs) were calculated between the hydrophobic surface (all

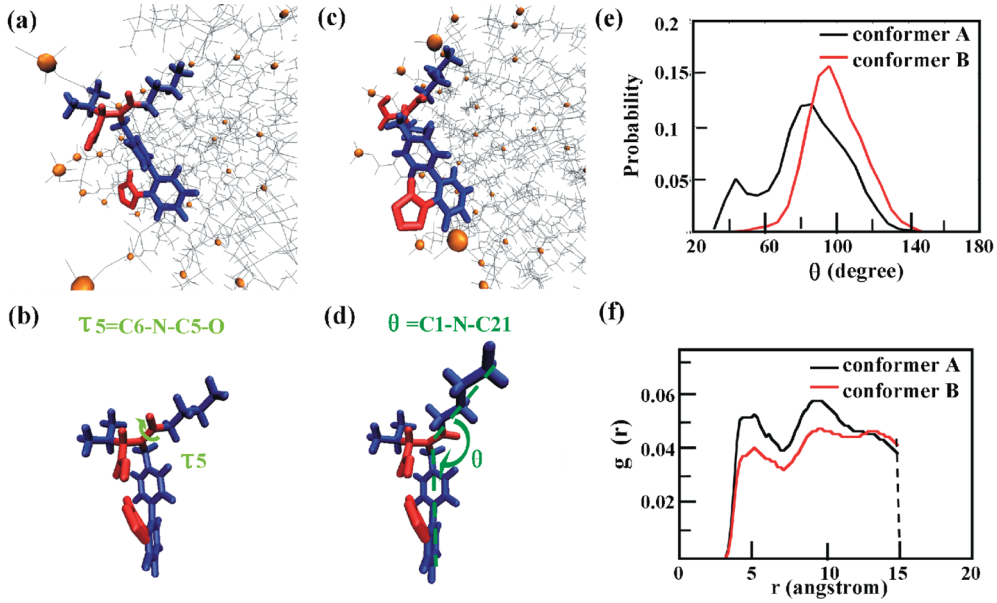

Figure 7. Simulation snapshots of VST: (a) conformer A in SDS micelle, (b) conformer A in vacuum, (c) conformer B in SDS micelle, and (d) conformer B in vacuum. The snapshots in SDS micelle were taken at 20 ns. Water molecules were not shown for clarity. VST is color-coded by hydrophobicity (blue) and hydrophilicity (red). SDS detergent tails are shown in gray bond format, and the sulfate head groups are shown as orange spheres. (e) The distribution of angle θ (C1−N−C21) of conformer A (black) and B (red) during the last 7 ns. (f) Radial distribution functions (RDFs) between the hydrophobic surface (all carbons in biphenyl and butyl of VST) and the hydrocarbon tails of SDS for the last 7 ns. The *x*-axis is distance in angstrom, and the RDFs were normalized by a density of 0.1. Hydrogen atoms were excluded from the calculation.

carbons in biphenyl and butyl of VST) and the hydrocarbon tails of SDS using trajectories over the last 7 ns. RDFs describe the probability of atoms found in a given distance from another specific atom or atom group, thus reflecting the strength of interaction. One can see from Figure 7(f) that the value of RDF of conformer A is overall larger than that of conformer B at short range. This result indicates that conformer A is closer to the SDS micelle core, and the concentrated hydrophobic surface facilitates the drug penetrating into the micelle.

During the simulation, the dihedral angles τ_3 and τ_4 of conformer B have been rotated to adapt for its final binding geometry in SDS. The isopropyl and terminal benzene become a little closer to generate better interactions with the micelle (Supporting Information, Figure S6a). Accompanied with this change, the tetrazole ring and carboxyl group of conformer B are further apart from each other (Supporting Information, Figure S6b). The twisted conformer B still has a more dispersive hydrophobic surface than conformer A, which could be responsible for its lower affinity to the micelles. Interestingly, Potamitis[11] has shown that two acidic groups of VST must be close to each other to contact well with the active site of the AT_1 receptor. In our simulation models, it is conformer A that matches this character, showing a reasonable higher binding affinity to SDS micelles.

Relative Binding Free Energy. In our experimental results, conformational exchange between conformer A and B is observed in the aqueous solution. The ratio of conformer A to B changes after the addition of SDS. To find which conformer is energetically preferable to bind with SDS, umbrella sampling simulations were carried out to calculate the relative binding free energy through a thermodynamic cycle. In Scheme 1, processes I and II ($\Delta G1$ and $\Delta G2$) are straightforward to measure experimentally but difficult to study by MD simulation. Therefore, processes III and IV ($\Delta G3$ and $\Delta G4$) are calculated instead.

The free energy profiles of VST isomerization from conformer A to B in aqueous solution and SDS micelle are shown in Figure

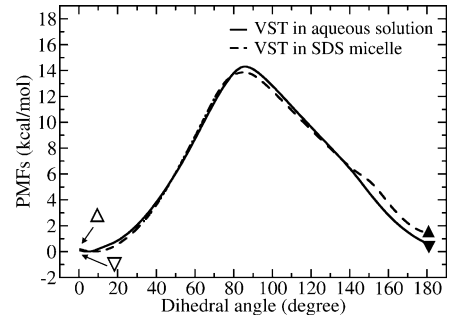

Figure 8. Potential of mean force (PMF) of VST in aqueous solution (conformer A ▽ and conformer B ▼) and in SDS micelle (conformer A △ and conformer B ▲). The isomerization undergoes a rotation of τ_5 from 0° to 180° corresponding to the conformational change from A to B.

8. Comparison of free energy curves along the simulation time shows that the PMFs are well converged (Supporting Information, Figure S7), which indicates that the simulations are long enough to minimize the statistical error. According to the Monte Carlo bootstrap analysis in WHAM, the error bars are found to be no more than 0.01 kcal/mol. In addition, the systematic error of PMF can be approximately canceled out by calculating the difference between $\Delta G3$ and $\Delta G4$, which makes the relative binding free energy reliable.

In aqueous solution, the isomerization free energy $\Delta G4$ is 0.59 kcal/mol (equal to 0.68 kcal/mol (▼) − 0.092 kcal/mol (▽)), while in SDS, the isomerization free energy $\Delta G3$ is 1.26 kcal/mol (equal to 1.45 kcal/mol (▲) − 0.19 kcal/mol (△)). According to Scheme 1, the calculated relative binding free energy $\Delta\Delta G_{(A\rightarrow B)}$ ($= \Delta G3 - \Delta G4 = \Delta G2 - \Delta G1$) is 0.67 kcal/mol which is positive. It means that the conformer B needs more free energy for binding, and thus conformer A is easier to bind with SDS.

Conclusions

The conformational properties of two VST conformers binding with SDS were analyzed using NMR spectroscopy

including proton chemical shifts, relaxation times, self-diffusion coefficients, and NOE measurements. The changes of NMR parameters indicate that both conformers interact with SDS, and conformer A exhibits a higher binding affinity. Molecular dynamics simulation results are in good agreement with the conclusions drawn by the experimental data. Comparison of the binding free energies for two conformers reveals that conformer A is energetically preferable.

Structural details revealed by both NOESY spectra and molecular dynamics simulations show that the butyl and biphenyl groups of VST are adjacent to the alkyl group of SDS, which indicate that the hydrophobic part of VST inserts into the center of the mimic membrane. Judging from the spatial structure, the hydrophobic part of conformer A is more centralized, while that of conformer B is relatively dispersive, which has been proved to be the primary reason why conformer A is energetically more favorable to interact with SDS.

In summary, the higher binding affinity of conformer A to SDS was addressed by the structural model established from the NMR experiments and MD simulation. It suggests that, in the living body, VST adopts a dominant conformation (conformer A) in the cell membrane before it reaches the AT_1 receptor. Investigations on the interactions between VST and the membrane mimicking environment reveal that the biological membrane plays an essential role in the stabilization of VST in its active state. The results should facilitate the understanding of functional mechanism of sartan drugs and provide insight into the drug design for hypertension treatment.

Acknowledgment. We wish to express our acknowledgement to Prof. Yuqi Feng (College of Chemistry and Molecular Sciences, Wuhan University) for providing us valsartan. We would like to thank Prof. Pei Zhou (Department of Biochemistry, Duke University Medical Center) for critical reading of the manuscript. This work is supported by grants from National Science Foundation of China (#20605026, #20635040, #90813017, and #20833007) and National Major Basic Research Program of China (#2009CB918603).

Supporting Information Available: Longitudinal relaxation times for valsartan protons in the absence and presence of SDS (Table S1); transverse relaxation times for valsartan protons in the absence and presence of SDS (Table S2); initial snapshot of VST simulation in SDS micelle (Figure S1); partial charges of VST calculated using the RESP methodology (Figure S2); distance between the center of mass of SDS micelle and VST (Figure S3); radial distribution function of sodium to sulfur of the SDS micelle (Figure S4); rmsd and rmsf of carbon atoms of VST relative to its initial structure (Figure S5); time profiles of distances between functional groups of VST (Figure S6); and free energies calculated from different total simulation times (Figure S7). This material is available free of charge via the Internet at http://pubs.acs.org.

References and Notes

(1) *The world health report 2002-Reducing Risks, Promoting Healthy Life*; Organization, W. H., Ed; WHO: Geneva, 2002.

(2) Kearney, P. M.; Whelton, M.; Reynolds, K.; Muntner, P.; Whelton, P. K.; He, J. *Lancet* **2005**, *365*, 217.

(3) Criscione, L.; Bradley, W. A.; Buhlmayer, P.; Whitebread, S.; Glazer, R.; Lloyd, P.; Mueller, P.; Gasparo, M. *Cardiovasc. Drug Rev.* **1995**, *13*, 230.

(4) Buhlmayer, P.; Furet, P.; Criscione, L.; de Gasparo, M.; Whitebread, S.; Schmidlin, T.; Lattmann, R.; Wood, J. *Bioorg. Med. Chem. Lett.* **1994**, *4*, 29.

(5) Mukoyama, M.; Nakajima, M.; Horiuchi, M.; Sasamura, H.; Pratt, R. E.; Dzau, V. J. *J. Biol. Chem.* **1993**, *268*, 24539.

(6) Murphy, T. J.; Alexander, R. W.; Griendling, K. K.; Runge, M. S.; Bernstein, K. E. *Nature* **1991**, *351*, 233.

(7) Sasaki, K.; Yamano, Y.; Bardhan, S.; Iwai, N.; Murray, J. J.; Hasegawa, M.; Matsuda, Y.; Inagami, T. *Nature* **1991**, *351*, 230.

(8) Goodfriend, T. L.; Elliott, M. E.; Catt, K. J. *N. Engl. J. Med.* **1996**, *334*, 1649.

(9) Ji, H.; Leung, M.; Zhang, Y.; Catt, K. J.; Sandberg, K. *J. Biol. Chem.* **1994**, *269*, 16533.

(10) Li, F.; Zhang, H. T.; Jiang, L.; Zhang, W. N.; Nie, J.; Feng, Y. Q.; Yang, M. H.; Liu, M. L. *Magn. Reson. Chem.* **2007**, *45*, 929.

(11) Potamitis, C.; Zervou, M.; Katsiaras, V.; Zoumpoulakis, P.; Durdagi, S.; Papadopoulos, M. G.; Hayes, J. M.; Grdadolnik, S. G.; Kyrikou, I.; Argyropoulos, D.; Vatougia, G.; Mavromoustakos, T. *J. Chem. Inf. Model.* **2009**, *49*, 726.

(12) Mavromoustakos, T.; Zoumpoulakis, P.; Kyrikou, I.; Zoga, A.; Siapi, E.; Zervou, M.; Daliani, I.; Dimitriou, D.; Pitsas, A.; Kamoutsis, C.; Laggner, P. *Curr. Top. Med. Chem.* **2004**, *4*, 445.

(13) Zoumpoulakis, P.; Daliani, I.; Zervou, M.; Kyrikou, I.; Siapi, E.; Lamprinidis, G.; Mikros, E.; Mavromoustakos, T. *Chem. Phys. Lipids* **2003**, *125*, 13.

(14) Bruch, M. D.; Rizo, J.; Gierasch, L. M. *Biopolymers* **1992**, *32*, 1741.

(15) Kloosterman, D. A.; Scahill, T. A.; Friendman, A. R. *J. Pept. Res.* **1993**, *6*, 211.

(16) McDonnel, P. A.; Opella, S. J. *J. Magn. Reson.* **1993**, *102*, 120.

(17) Parker, W.; Song, P. S. *Biophys. J.* **1992**, *61*, 1435.

(18) Moroi, Y. *J. Colloid Interface Sci.* **1988**, *122*, 308.

(19) Cui, Y.; Wen, J.; Hung Sze, K.; Man, D.; Lin, D.; Liu, M.; Zhu, G. *Anal. Biochem.* **2003**, *315*, 175.

(20) McCoy, M. A.; Wyss, D. F. *J. Am. Chem. Soc.* **2002**, *124*, 2104.

(21) Medek, A.; Hajduk, P. J.; Mack, J.; Fesik, S. W. *J. Am. Chem. Soc.* **2000**, *122*, 1241.

(22) Yang, Y.; Bai, G.; Zhang, X.; Ye, C.; Liu, M. *Anal. Biochem.* **2004**, *324*, 292.

(23) Bai, G.; Cui, Y.; Yang, Y.; Ye, C.; Liu, M. *J. Pharmaceut. Biomed.* **2005**, *38*, 588.

(24) Liu, M. L.; Nicholson, J. K.; Lindon, J. C. *Anal. Commun.* **1997**, *34*, 225.

(25) Delfini, M.; Gianferri, R.; Dubbini, V.; Manetti, C.; Gaggelli, E.; Valensin, G. *J. Magn. Reson.* **2000**, *144*, 129.

(26) Veglia, G.; Delfini, M.; Giudice, M. R. D.; Gaggelli, E.; Valensin, G. *J. Magn. Reson.* **1998**, *130*, 281.

(27) Hajduk, P. J.; Olejniczak, E. T.; Fesik, S. W. *J. Am. Chem. Soc.* **1997**, *119*, 12257.

(28) Liu, M.; Nicholson, J. K.; Parkinson, J. A.; Lindon, J. C. *Anal. Chem.* **1997**, *69*, 1504.

(29) Luo, R. S.; Liu, M. L.; Mao, X. A. *Spectrochim. Acta, Part A* **1999**, *55A*, 1897.

(30) Chen, A.; Shapiro, M. J. *J. Am. Chem. Soc.* **1998**, *120*, 10258.

(31) Meyer, B.; Weimar, T.; Peters, T. *Eur. J. Biochem.* **1997**, *246*, 705.

(32) Nie, J.; Xiang, B. R.; Feng, Y. Q.; Wang, D. H. *J. Liq. Chromatogr. Relat. Technol.* **2006**, *29*, 553.

(33) Zhang, X.; Li, C.; Ye, C.; Liu, M. L. *Anal. Chem.* **2001**, *73*, 3528.

(34) Case, D. A.; Darden, T.; Cheatham, T. E., III.; Simmerling, C. L.; Wang, J.; Duke, R.; Luo, R.; Merz, K. M., Jr.; Wang, B.; Pearlman, D. A.; Crowley, M.; Brozell, S.; Tsui, V.; Gohlke, H.; Mongan, J.; Hornak, V.; Cui, G.; Beroza, P.; Schafmeister, C.; Caldwell, J. W.; Ross, W. S.; Kollman, P. A. *AMBER 9.0*; University of California, San Francisco: San Francisco, CA, 2006.

(35) Wang, J.; Wolf, R. M.; Caldwell, J. W.; Kollman, P. A.; Case, D. A. *J. Comput. Chem.* **2004**, *25*, 1157.

(36) Chen, J. M.; Su, T. M.; Mou, C. Y. *J. Phys. Chem.* **1986**, *90*, 2418.

(37) Khandelia, H.; Kaznessis, Y. N. *Peptides* **2005**, *26*, 2037.

(38) Jorgensen, W. L.; Chandrasekhar, J.; Madura, J. D.; Impey, R. W.; Klein, M. L. *J. Chem. Phys.* **1983**, 79.

(39) Khandelia, H.; Kaznessis, Y. N. *J. Phys. Chem. B* **2007**, *111*, 242.

(40) Frisch, M J.; Trucks, G. W.; Schlegel, H. B.; Scuseria, G. E.; Robb, M. A.; Cheeseman, J. R.; Montgomery, J. A., Jr.; Vreven, T.; Kudin, K. N.; Burant, J. C.; Millam, J. M.; Iyengar, S. S.; Tomasi, J.; Barone, V.; Mennucci, B.; Cossi, M.; Scalmani, G.; Rega, N.; Petersson, G. A.; Nakatsuji, H.; Hada, M.; Ehara, M.; Toyota, K.; Fukuda, R.; Hasegawa, J.; Ishida, M.; Nakajima, T.; Honda, Y.; Kitao, O.; Nakai, H.; Klene, M.; Li, X.; Knox, J. E.; Hratchian, H. P.; Cross, J. B.; Bakken, V.; Adamo, C.; Jaramillo, J.; Gomperts, R.; Stratmann, R. E.; Yazyev, O.; Austin, A. J.; Cammi, R.; Pomelli, C.; Ochterski, J. W.; Ayala, P. Y.; Morokuma, K.; Voth, G. A.; Salvador, P.; Dannenberg, J. J.; Zakrzewski, V. G.; Dapprich, S.; Daniels, A. D.; Strain, M. C.; Farkas, O.; Malick, D. K.; Rabuck, A. D.; Raghavachari, K.; Foresman, J. B.; Ortiz, J. V.; Cui, Q.; Baboul, A. G.; Clifford, S.; Cioslowski, J.; Stefanov, B. B.; Liu, G.; Liashenko, A.; Piskorz, P.; Komaromi, I.; Martin, R. L.; Fox, D. J.; Keith, T.; Al-Laham, M. A.; Peng, C. Y.; Nanayakkara, A.; Challacombe, M.; Gill, P. M. W.; Johnson, B.; Chen, W.; Wong, M. W.; Gonzalez, C.; Pople, J. A. *Gaussian 03*, B.05 ed.; Gaussian, Inc.: Pittsburgh, PA, 2003.

(41) Fox, T.; Kollman, P. A. *J. Phys. Chem. B* **1998**, *102*, 8070.
(42) Berendsen, H. J. C.; Postma, J. P. M.; Vangunsteren, W. F.; Dinola, A.; Haak, J. R. *J. Chem. Phys.* **1984**, *81*, 3684.
(43) Darden, T.; York, D.; Pedersen, L. *J. Chem. Phys.* **1993**, *98*, 10089.
(44) Ryckaert, J. P.; Ciccotti, G.; Berendsen, H. J. C. *J. Comput. Phys.* **1977**, *23*, 327.
(45) Humphrey, W.; Dalke, A.; Schulten, K. *J. Mol. Graph.* **1996**, *14*, 33.
(46) Lybrand, T. P.; McCammon, J. A.; Wipff, G. *Proc. Natl. Acad. Sci. U.S.A.* **1986**, *83*, 833.
(47) Torrie, G. M.; Valleau, J. P. *Chem. Phys. Lett.* **1974**, *28*, 578.
(48) Brooks, C. L., III.; Karplus, M.; Pettitt, B. M. *Proteins: A Theoretical Perspective of Dynamics, Structure, and Thermodynamics*, 2nd ed.; John Wiley & Sons, Inc., 1988.
(49) Kumar, S.; Rosenberg, J. M.; Bouzida, D.; Swendsen, R. H.; Kollman, P. A. *J. Comput. Chem.* **1995**, *16*, 1339.
(50) Roux, B. *Comput. Phys. Commun.* **1995**, *91*, 275.
(51) Grossfield, A. An implementation of WHAM: the Weighted Histogram Analysis Method, http://dasher.wustl.edu/alan/, 2004.
(52) Flesch, G.; Muller, P.; Lloyd, P. *Eur. J. Clin. Pharmacol.* **1997**, *52*, 115.
(53) Bendedouch, D.; Chen, S. H.; Koehler, W. C. *J. Phys. Chem.* **1983**, *87*, 153.
(54) Gao, J.; Ge, W.; Hu, G. H.; Li, J. H. *Langmuir* **2005**, *21*, 5223.
(55) Bruce, C. D.; Berkowitz, M. L.; Perera, L.; Forbes, M. D. E. *J. Phys. Chem. B* **2002**, *106*, 3788.

JP908958K